New stable ternary alkaline-earth metal Pb(II) oxides: Ca/Sr/$BaPb_2O_3$ and $BaPbO_2$

Yuwei Li,[1,2] Lijun Zhang,[2,*] and David J. Singh[1,†]

[1]*Department of Physics and Astronomy, University of Missouri, Columbia, Missouri 65211-7010 USA*

[2]*Key Laboratory of Automobile Materials of MOE and College of Materials Science and Engineering, Jilin University, Changchun 130012, China*

(Received 27 July 2017; published 16 October 2017)

The different but related chemical behaviors of Pb(II) oxides compared to Sn(II) oxides, and the existence of known alkali/alkali-earth metal Sn(II) ternary phases, suggest that there should be additional ternary Pb(II) oxide phases. Here, we report structure searches on the ternary alkaline-earth metal Pb(II) oxides leading to four new phases. These are two ternary Pb(II) oxides, $SrPb_2O_3$ and $BaPb_2O_3$, which have larger chemical potential stability ranges compared with the corresponding Sn(II) oxides, and additionally two other ternary Pb(II) oxides, $CaPb_2O_3$ and $BaPbO_2$, for which there are no corresponding Sn(II) oxides. Those Pb(II) oxides are stabilized by Pb-rich conditions. These structures follow the Zintl behavior and consist of basic structural motifs of $(PbO_3)^{4-}$ anionic units separated and stabilized by the alkaline-earth metal ions. They show wide band gaps ranging from 2.86 to 3.12 eV, and two compounds ($CaPb_2O_3$ and $SrPb_2O_3$) show rather light hole effective masses (around $2m_0$). The valence band maxima of these compounds have a Pb-6*s*/O-2*p* antibonding character, which may lead to *p*-type defect (or doping) tolerant behavior. This suggests alkaline-earth metal Pb(II) oxides may be potential *p*-type transparent conducting oxides.

DOI: 10.1103/PhysRevMaterials.1.055001

I. INTRODUCTION

Allred noted early on that the electronegativity of tetravalent Pb is anomalous, and in particular is anomalously higher than that of tetravalent Sn [2.33 for Pb(IV) vs 1.96 for Sn(IV)] [1]. This is a consequence of the relativistic contraction of the Pb valence *s* state. This stabilizes the Pb^{2+} valence, and is an important aspect of the chemistry of Pb. Additionally, the spin-orbit interaction lowers the energy of the valence $p_{1/2}$ state of Pb, which raises the electronegativity of Pb(II), though to a lesser extent, but again leading to higher electronegativity for Pb than Sn [1.87 for Pb(II) vs 1.80 for Sn(II), with the Allred data], again opposite to the usual trend of decreasing electronegativity down a column of the periodic table. This has important implications for the chemical properties, for example, reducing the reactivity of metallic Pb, and making Pb(II) oxides relatively more stable and common than Sn(II) oxides. The standard enthalpies of formation [2] of PbO and PbO_2 are relatively similar, −219.41 and −274.47 kJ/mol, which in the solid state means that PbO is stable. The corresponding values for SnO and SnO_2 are −280.71 and −577.63 kJ/mol [3], which means that SnO is marginally unstable against separation into Sn and SnO_2, complicating the synthesis and use of SnO in applications. This stability of Pb(II) oxides is important for applications of Pb compounds, such as in the electroactive Pb perovskite oxides [e.g., $Pb(Zr,Ti)O_3$] and the halide solar absorbers (e.g., $CH_3NH_3PbI_3$). These differences also have important effects for the electronic properties of the compounds.

Turning to the ternary oxide phases with electropositive elements, we note that many alkali metal and alkaline-earth metal Sn(II) oxides have been reported under ambient conditions, include $Na_2Sn_2O_3$, $K_2Sn_2O_3$ [4,5], and at least in a narrow chemical potential window, based on density functional calculations [6], $SrSn_2O_3$ and $BaSn_2O_3$. The higher stability of Pb(II) compared to Sn(II) suggests that related compounds may exist for the Pb case, possibly with broader stability windows. However, data on such phases for the alkaline-earth metal Pb(II) oxides are lacking.

Here, we report a systematic investigation of such possible phases, $M_mPb_nO_{m+n}$, M = Mg, Ca, Sr, and Ba, m,n = 1,2. Our study is based on first-principles crystal structure prediction methods using unbiased global optimization. The most challenging issue associated with these Pb(II) ternary oxides is whether they are thermodynamically stable relative to the strongly competing Pb(II) and Pb(IV) compounds such as PbO, PbO_2, Ca/Mg/Sr/$BaPbO_3$, and the stable alkaline-earth metal oxides. We find (1) in $MPbO_2$ systems, only the large electropositive Ba ion stabilizes the ternary oxide, $BaPbO_2$, against decomposing into competing phases in Pb-rich conditions; (2) in MPb_2O_3 systems, M = Ca, Sr, and Ba stabilize ternary Pb(II) oxides, but Mg does not; (3) in M_2PbO_3 systems, no alkaline-earth metal element stabilizes these with respect to competing phases. This is into the alkaline-earth metal Sn(II) oxides, where only $SrSn_2O_3$ and $BaSn_2O_3$ are stable and the chemical conditions for this are narrow due to competing phases. We additionally find the stable phases of Ca/Sr/$BaPb_2O_3$ and $BaPbO_2$ have reasonably dispersive valence bands (VBs) with moderate hole effective transport masses m_h^*, leading to an expectation of reasonably high hole mobility.

II. COMPUTATIONAL METHODS

The identification of new phases based on density functional calculations without *a priori* knowledge of the crystal structures is a longstanding challenge that has been addressed relatively recently using global optimization methods [7]. We searched for stable crystal structures of $M_mPb_nO_{m+n}$ using the particle swarm evolution algorithm and random algorithm

*lijun_zhang@jlu.edu.cn

†singhdj@missouri.edu

up to 24 atoms per unit cell as implemented in the CALYPSO code [8,9]. The key feature of this type of structure search method is the ability to rapidly identify ground-state and metastable structures with only knowledge of the chemical composition. Details of the algorithm and applications have been discussed elsewhere [10–13]. We used the projector augmented-wave (PAW) method [14] as implemented in the VASP code [15] with the generalized gradient approximation of Perdew, Burke, and Ernzerhof (PBE-GGA) [16] for the density functional calculations in the crystal structure prediction. This code provides reliable total energies and has efficient structure optimization, including optimization of the cell shape using the stress tensor. The $5d^{10}6s^26p^2$ (Pb), $2s^22p^4$ (O), $3s^2$ (Mg), $3p^64s^2$ (Ca), $4s^24p^65s^2$ (Sr), and $5s^25p^66s^2$ (Ba) states were treated as valence electrons of PAW pseudopotentials. We used medium-quality computational parameters to evaluate relative energies of explored structures and accelerate structure searches. Then the low-lying energy structures were further optimized with more accurate computational parameters, e.g., kinetic energy cutoff of 520 eV and k-point meshes with a grid spacing of $2\pi \times 0.032$ Å^{-1}. These settings generally ensure convergence of total energies at the level of 1 meV per atom. We checked the dynamical stability of the predicted phases by computing the phonon dispersions. This is important because the unit cell size is limited in the structure search (we allowed up to 24 atoms per cell), and this can potentially mask a dynamical instability of the predicted structure that would lead to a larger unit cell. For this purpose, we calculated phonon dispersions by the supercell finite difference method as implemented in the PHONOPY code [17].

Standard density functionals, such as the PBE-GGA, are designed to produce accurate total energies, but do not in general predict reliable electronic structure features, such as band gaps. We did band structure, density of states (DOS), and optical calculations using the modified Becke-Johnson (mBJ) potential of Tran and Blaha [18]. This potential gives band gaps in remarkably good accord with experiment for a wide variety of simple semiconductors and insulators [18–22]. For this purpose, we used the linearized augmented plane-wave (LAPW) method [23] as implemented in the WIEN2K code [24]. This code has an accurate implementation of the mBJ potential, and accurate treatments of relativistic effects on the band structure. Spin-orbit coupling (SOC) was included in the electronic structures, optical properties, and effective mass calculations, as the $^3P_0$-$^3P_2$ spin-orbit splitting is very large for Pb (1.32 eV) [25,26]. The calculations were done using the structures and lattice parameters generated in a structure search. We used LAPW sphere radii of 2.14, 2.2, and 1.85 bohrs for Ca, Pb, and O in $CaPb_2O_3$, 2.25, 2.29, and 1.87 bohrs for Sr, Pb, and O in $SrPb_2O_3$, 2.46, 2.27, and 1.88 bohrs for Ba, Pb, and O in $BaPb_2O_3$, and 2.40, 2.24, and 1.83 bohrs for Ba, Pb, and O in $BaPbO_2$, respectively. A basis set cutoff k_{max} determined by the criterion $R_{min}k_{max} = 9.0$ was used. Here, R_{min} is the O sphere radius. The optical properties were obtained for electric dipole transitions neglecting local field effects using the optical package of WIEN2K code. We also calculated transport effective masses for the compounds to provide insight into their potential conductivity if doped. These were calculated through the semiclassical Boltzmann transport theory, at 300 K, as the effective mass that in a single parabolic band model would yield the same σ/τ as obtained from the actual band structure [27]. This takes into account the effects of nonparabolicity and anisotropy, multiple bands, etc., on carrier transport.

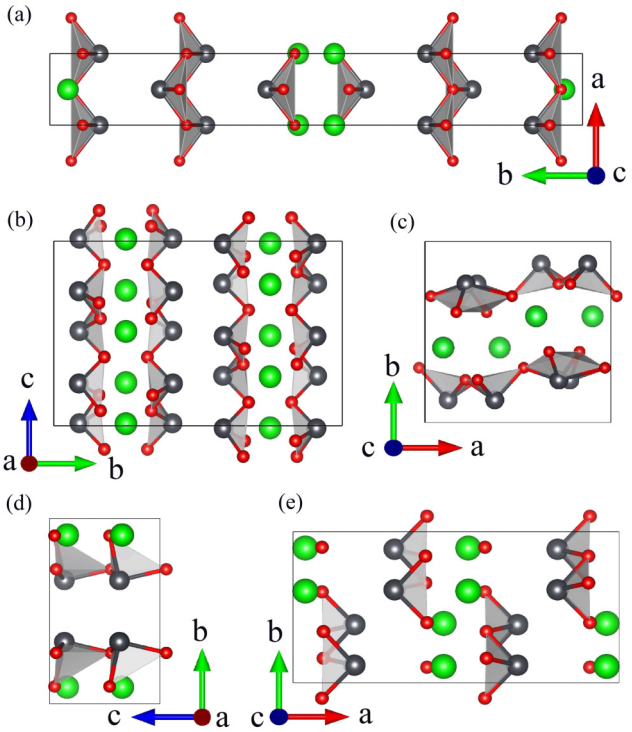

FIG. 1. Lowest-energy structures of (a) $MgPb_2O_3$, (b) $Ca/SrPb_2O_3$, (c) $BaPb_2O_3$, (d) $MgPbO_2$, (e) $Ca/Sr/BaPbO_2$ as identified by a structure search. Gray spheres represent Pb atoms, red spheres represent O atoms, and bright green spheres represent alkaline-earth metal atoms.

III. RESULTS AND DISCUSSION

We begin with the stable compounds from the structure searches. The lowest-energy structures of MPb_2O_3 and $MPbO_2$ as found in our structure searches are shown in Fig. 1. Detailed structural information is given in Table I. Data for the M_2PbO_3 compounds, which are not stable as seen below, identified are given in the Supplemental Material, Fig. S1 and Table S1 [28]. The role of electropositive alkaline-earth metals is to donate electrons and stabilize lattices via the Madelung potential. Therefore, in general, these compounds can be regarded as Zintl phase materials [29].

In $MPbO_2$ systems, all materials are layered. In MPb_2O_3 systems, the basic motif of $MgPb_2O_3$ is a PbO_4 polyhedron in which Pb is fourfold coordinated by O. However, in $Ca/Sr/BaPb_2O_3$, Pb is threefold coordinated by O and forming PbO_3 structural units, which are connected to form layers. In M_2PbO_3 systems, there are different kinds of Pb-O coordinations: PbO_6 octahedrons in Ca_2PbO_3 [these share edges to form three-dimensional (3D) structures], PbO_4 polyhedra in Mg_2PbO_3 and Sr_2PbO_3, which connect to form two-dimensional (2D) layered structures, and PbO_3 isolated

TABLE I. Structural data for the lowest-energy structures of $M\mathrm{Pb_2O_3}$ and $M\mathrm{PbO_2}$ (M = Mg, Ca, Sr, Ba) identified from structure searches.

Space group	Lattice parameters (Å)	Wyckoff positions	Atoms	x	y	z
			Mg	0.5000	0.9661	0.7500
			Pb1	0.5000	0.7929	0.7500
$MgPb_2O_3$	$a = 3.0756$	4c	Pb2	0.0000	0.9072	0.2500
$Cmcm$	$b = 27.6019$		O1	0.5000	0.0402	0.7500
	$c = 4.3844$		O2	0.0000	0.0616	0.2500
			O3	0.5000	0.7566	0.2500
		4c	Ca1	0.2500	0.2500	0.5113
		4d	Ca2	0.2500	0.7500	0.2661
$CaPb_2O_3$	$a = 5.7303$	8e	Pb1	0.3306	0.9107	0.9860
$Pccn$	$b = 16.3264$	8e	Pb2	0.3399	0.4129	0.2291
	$c = 10.3165$	8e	O1	0.9672	0.6571	0.8333
		8e	O2	0.9674	0.1620	0.0814
		8e	O3	0.5016	0.6754	0.6274
		4c	Sr1	0.2500	0.2500	0.0061
		4d	Sr2	0.2500	0.7500	0.7576
$SrPb_2O_3$	$a = 5.9366$	8e	Pb1	0.3422	0.9138	0.4749
$Pccn$	$b = 16.8413$	8e	Pb2	0.3504	0.4160	0.7210
	$c = 10.3873$	8e	O1	0.9517	0.6547	0.3289
		8e	O2	0.9535	0.1589	0.5789
		8e	O3	0.5016	0.6629	0.1264
			Ba	0.9016	0.5866	0.1953
			Pb1	0.2796	0.7656	0.2646
$BaPb_2O_3$	$a = 9.4328$	4a	Pb2	0.3753	0.1244	0.6230
$Pca2_1$	$b = 9.2801$		O1	0.2824	0.2355	0.9103
	$c = 6.1786$		O2	0.8317	0.3910	0.5364
			O3	0.5318	0.3022	0.5588
	$a = 5.6763$		Mg	0.0708	0.0893	0.8419
$MgPbO_2$	$b = 8.9200$	4a	Pb	0.4687	0.6667	0.3661
$Pca2_1$	$c = 5.1311$		O1	0.5962	0.9072	0.4551
			O2	0.4083	0.7259	0.9414
	$a = 14.078$		Ca	0.9622	0.3924	0.2581
$CaPbO_2$	$b = 6.8089$	8c	Pb	0.8117	0.8841	0.2444
$Pbca$	$c = 5.8669$		O1	0.9064	0.6614	0.0525
			O2	0.5889	0.6025	0.1226
	$a = 14.1953$		Sr	0.9516	0.4027	0.7534
$SrPbO_2$	$b = 7.2384$	8c	Pb	0.8108	0.8789	0.7359
$Pbca$	$c = 6.0483$		O1	0.9021	0.6809	0.5331
			O2	0.5923	0.5959	0.6421
	$a = 14.9006$		Ba	0.4410	0.4235	0.7498
$BaPbO_2$	$b = 7.5243$	8c	Pb	0.3140	0.8815	0.7254
$Pbca$	$c = 6.1941$		O1	0.3985	0.7145	0.4998
			O2	0.0924	0.5969	0.6699

units in Ba_2PbO_3. The different kinds of Pb-O coordinations can be rationalized in terms of the amount and atomic radius of Mg, Ca, Sr, and Ba, where large volumes occupied by the metal ions works against connections of the Pb-O polyhedra.

For thermodynamic stability of $M_m\mathrm{Pb}_n\mathrm{O}_{m+n}$ structures three criteria should be satisfied: (1) $m\Delta\mu_M + n\Delta\mu_{\mathrm{Pb}} + (m+n)\Delta\mu_{\mathrm{O}} = \Delta H_f(M_m\mathrm{Pb}n\mathrm{O}_{m+n})$, (2) $\Delta\mu_i \leqslant 0$ ($i = M$,Pb,O), and (3) $n_j\Delta\mu_M + m_j\Delta\mu_{\mathrm{Pb}} + q_j\Delta\mu_{\mathrm{O}} \leqslant \Delta H_f(M_{n_j}\mathrm{Pb}m_j\mathrm{O}_{q_j})$, $j = 1,\ldots,t$, where $\Delta\mu_i = \mu_i - \mu_i^0$ is the deviation of actual chemical potential of atomic species i during growth (μ_i) from that of the bulk elemental solid or gas phase (μ_i^0), ΔH_f is the heat of formation, and $M_{n_j}\mathrm{Pb}m_j\mathrm{O}_{q_j}$ represents all known j competing phases. These competing phases limit the size of the stable region. Condition (1) is for equilibrium growth, condition (2) is to prevent precipitation to elemental phases of atomic species, and condition (3) is the stability against competing phases. Figure 2 shows two-dimensional phase stability diagrams with two independent quantities with $\Delta\mu_M$ and $\Delta\mu_{\mathrm{Pb}}$ as variables. For each case, all competing binary and ternary compounds are considered. As seen, there are stable regions for $\mathrm{Ca/Sr/BaPb_2O_3}$ and $\mathrm{BaPbO_2}$, especially under Pb-rich conditions (i.e., $\Delta\mu_{\mathrm{Pb}}$ close to zero). The other compounds do not show stability.

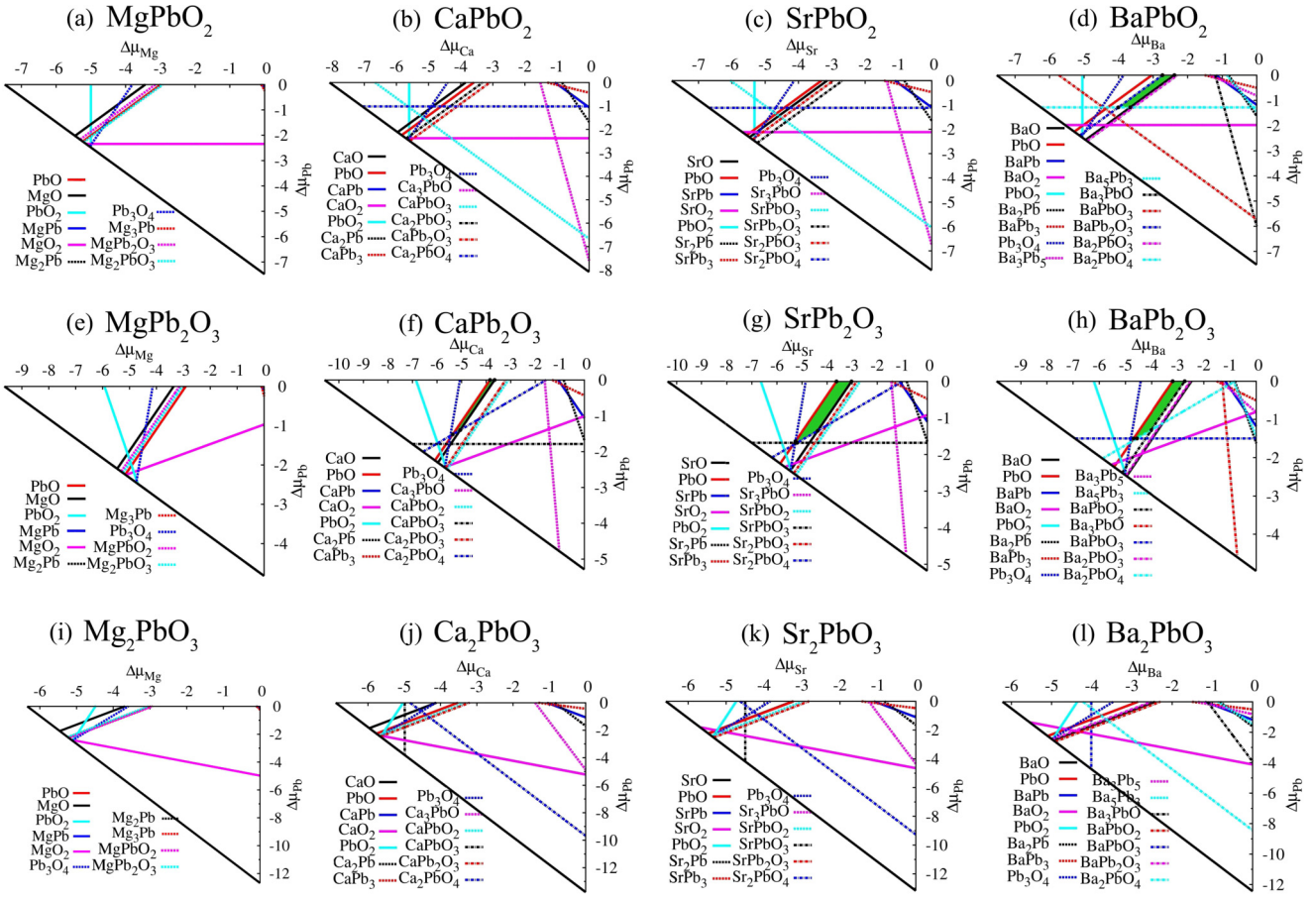

FIG. 2. Phase stability diagrams for (a) $MgPbO_2$, (b) $CaPbO_2$, (c) $SrPbO_2$, (d) $BaPbO_2$, (e) $MgPb_2O_3$, (f) $CaPb_2O_3$, (g) $SrPb_2O_3$, (h) $BaPb_2O_3$, (i) Mg_2PbO_3, (j) Ca_2PbO_3, (k) Sr_2PbO_3, and (l) Ba_2PbO_3, respectively. Each line represents a known competing phase; the stable region, if any, is indicated in green.

As expected, the important competition is from binary PbO and Ca/SrO for $CaPb_2O_3$ and $SrPb_2O_3$, as seen in Figs. 2(f) and 2(g). The important competing phases for $BaPbO_2$ are $BaPb_2O_3$ and BaO, and for $BaPb_2O_3$ they are $BaPbO_2$ and PbO. Compared with alkaline-earth metal Sn(II) oxides, alkaline-earth metal Pb(II) oxides have larger stable regions, e.g., in Sr/$BaPb_2O_3$, and have much more stable compounds, such as $BaPbO_2$ and $CaPb_2O_3$.

In addition to the thermodynamic stability with respect to competing phases, we have also examined the lattice dynamical stability of the predicted Ca/Sr/$BaPb_2O_3$ and $BaPbO_2$ phases. Figure 3 shows the phonon dispersion curves. The absence of any imaginary phonon modes indicated the dynamical stability of these structures. These results indicate that by controlling the chemical potentials of the reactants, it should be possible to grow Ca/Sr/$BaPb_2O_3$ and $BaPbO_2$.

Figure 4 shows calculated band gaps and direction-dependent (x, y, and z) and average effective masses. The average effective masses are calculated as the direction average relevant for conductivity, $1/m^* = (1/m_x^* + 1/m_y^* + 1/m_z^*)/3$, for the predicted lowest-energy structures of Ca/Sr/$BaPb_2O_3$ and $BaPbO_2$. These compounds show direct or quasidirect band gaps, along with larger direct gaps of approximately 3 eV. The direct gaps of the stable compounds, Ca/Sr/$BaPb_2O_3$ and $BaPbO_2$, are 2.99, 3.09, 2.91, and 3.16 eV, respectively.

As seen, $CaPb_2O_3$ and $SrPb_2O_3$ have moderate m_e^* and m_h^*. $BaPb_2O_3$ and $BaPbO_2$ have very low m_e^* and a heavier m_h^*. Their valence bands dispersions (or m_h^*) come from O $2p$ states with some Pb $6s$ hybridization. Large Pb-O-Pb angles maximize the overlap for this hopping channel, providing dispersion and reduction of the m_h^*. Also, there is a large anisotropy of the m^*, as seen in Fig. 4(b). This is a consequence of the layered structures. The absorption spectra, which may be useful for characterizing the electronic structure in relation to experiment if the compounds are synthesized, are shown in Fig. 5.

We note that the complex layered structures, with relatively low-frequency phonons and the heavy Pb atoms, may lead to low thermal conductivity. The compounds also show complex band structures near the band extrema, specifically for p-type, multiple bands within 0.2 eV, multiple carrier pockets, and nonparabolic shapes. The combination of low thermal conductivity and complex bands is favorable for thermoelectric performances [30,31]. As such, if synthesized, it will be of interest to investigate these compounds in this context.

$K_2Pb_2O_3$ has been suggested as a potential p-type transparent conductor. The gaps that we find for the stable alkaline-earth metal compounds are higher than those of both PbO [32] and $K_2Pb_2O_3$ [33], which should lead to better transparency over the visible spectrum. Turning to the effective masses, both $CaPb_2O_3$ and $SrPb_2O_3$ show reasonably low effective

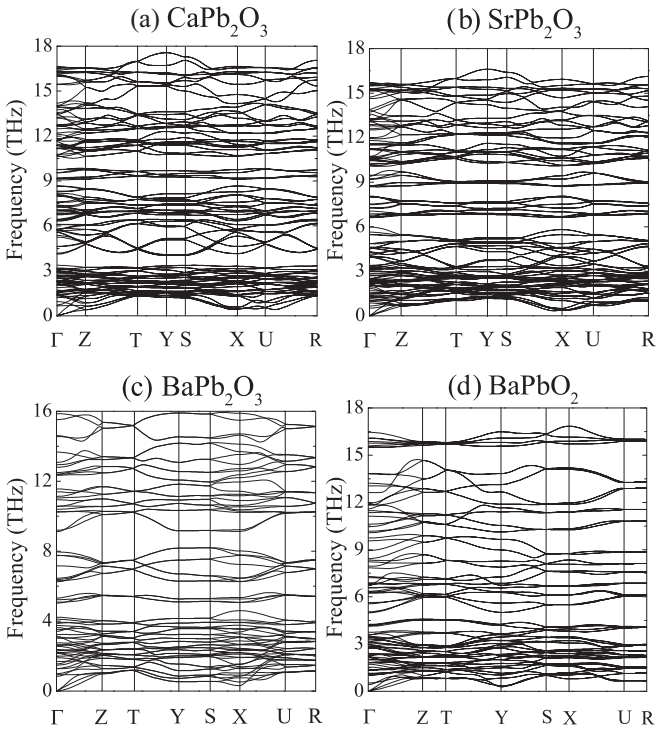

FIG. 3. Calculated phonon dispersion curves of (a) *Pccn*-$CaPb_2O_3$, (b) *Pccn*-$SrPb_2O_3$, (c) *Pca*2$_1$-$BaPb_2O_3$, and (d) *Pbca*-$BaPbO_2$ structures.

masses for holes (m_h^*), $1.89m_0$ and $2.25m_0$, respectively, comparable to the effective masses of electrons. The low m_h^* values are comparable to those of $K_2Pb_2O_3$ and other *p*-type

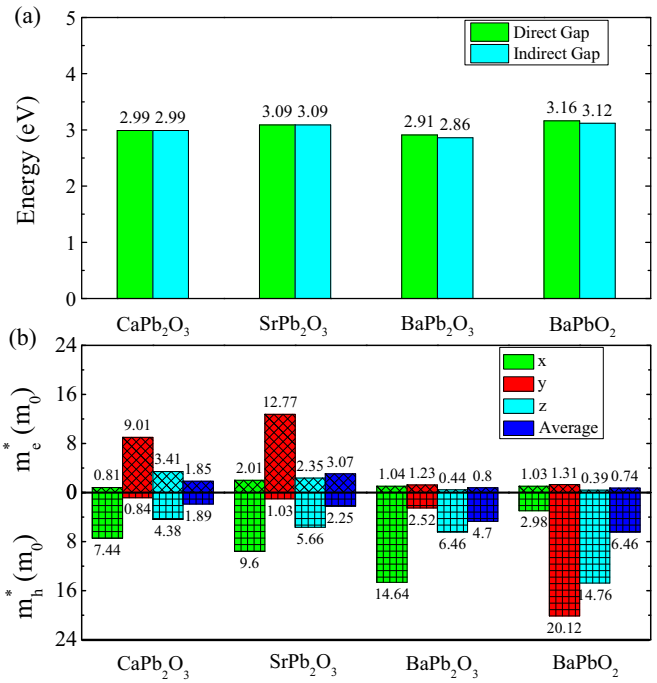

FIG. 4. (a) Calculated direct/indirect band gaps and direction-dependent (x, y, and z) and (b) average effective masses of electrons (m_e^*) and holes (m_h^*) for Ca/Sr/$BaPb_2O_3$ and $BaPbO_2$.

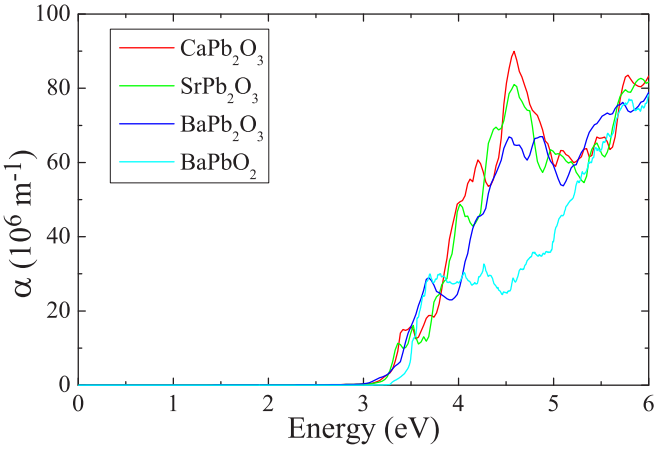

FIG. 5. Absorption spectra for $CaPb_2O_3$ (black), $SrPb_2O_3$ (red), $BaPb_2O_3$ (blue), and $BaPbO_2$ (cyan).

transparent conducting oxides (TCOs) candidates proposed in Ref. [33]. Based on the often similar properties of Ca, Sr, and Ba oxides and the common motif of PbO_3 units making up Ca/Sr/$BaPb_2O_3$ and $BaPbO_2$, one may suppose that $BaPb_2O_3$ and $BaPbO_2$ will show electronic properties similar to Ca/$SrPb_2O_3$. However, in fact, $BaPb_2O_3$ and $BaPbO_2$ show a heavy m_h^*, $4.70m_0$ and $6.46m_0$, respectively, as seen in Fig. 4(b), which originates from its weakly dispersing top valence bands.

Figures 6 and 7 show band structures and projected DOS for these four stable compounds: Ca/Sr/$BaPb_2O_3$ and $BaPbO_2$. As mentioned, the band gaps of these ternary compounds are

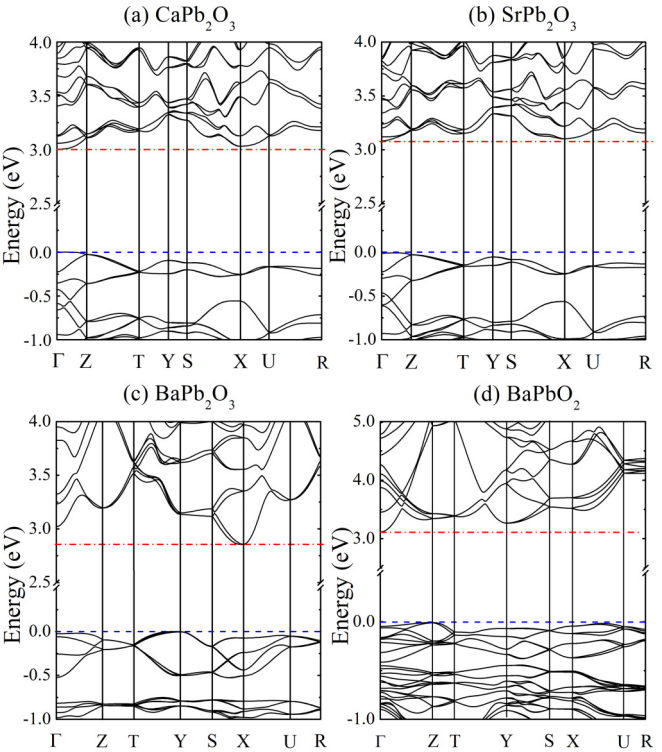

FIG. 6. Band structures of (a) $CaPb_2O_3$, (b) $SrPb_2O_3$, (c) $BaPb_2O_3$, and (d) $BaPbO_2$. The VB maximum is set to energy zero.

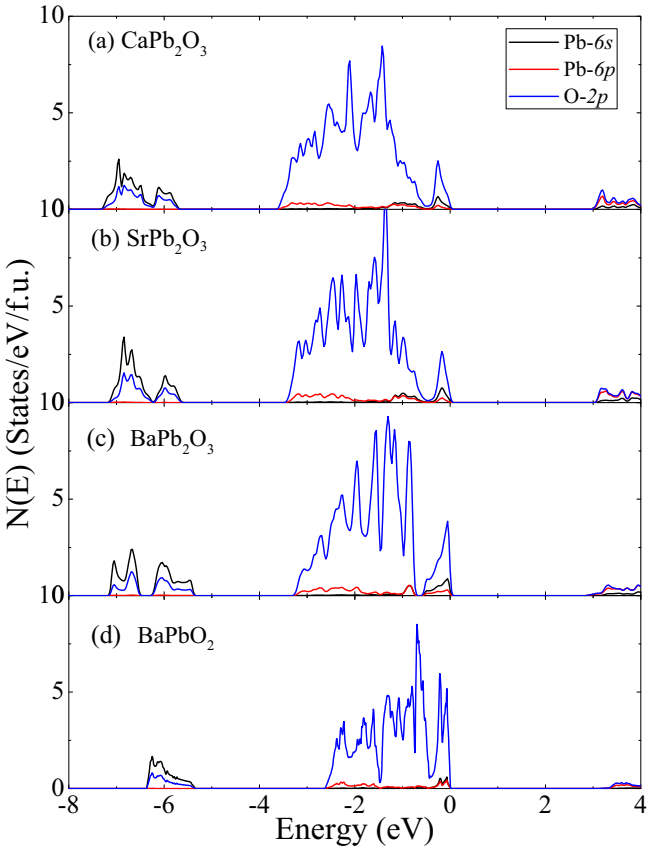

FIG. 7. Projected DOS of (a) $CaPb_2O_3$, (b) $SrPb_2O_3$, (c) $BaPb_2O_3$, and (d) $BaPbO_2$ onto the atomic orbitals of Pb-6s (black lines), Pb-6p (red lines), and O-2p (blue lines), respectively. The energy zero is at the valence band maximum.

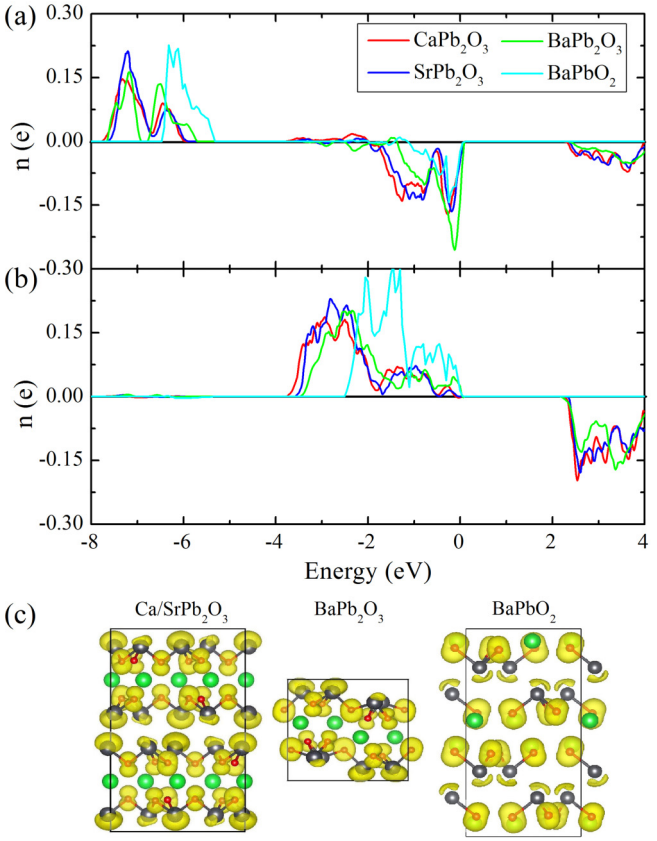

FIG. 8. Crystal orbital overlap population (COOP) between (a) Pb-6s and O-2p and (b) Pb-6p and O-2p orbitals for $CaPb_2O_3$ (red lines), $SrPb_2O_3$ (blue lines), $BaPb_2O_3$ (green lines), and $BaPbO_2$ (cyan lines). Positive $n(e)$ represents bonding states and negative $n(e)$ represents antibonding ones. The VB maximum is set to energy zero. Decomposed charge density for the VB maximum of each material is shown in (c).

significantly widened relative to binary PbO. This reflects the stabilization of the Pb^{2+} state relative to Pb by the Ewald potential in these structures. This leads to an upward shift of the Pb states relative to the O states. Since the valence bands are O p derived and the conduction bands are Pb p derived, this increases the band gap.

The crystal orbital overlap population (COOP) [34] is shown in Figs. 8(a) and 8(b). These are obtained with the VASP code using the PBE-GGA functional. There are Pb-6s/O-2p antibonding states mainly at -2 to 0 eV for them, as seen in Fig. 8(a). Besides, there are strong Pb-6p/O-2p bonding states at -4 to 0 eV for them, as seen in Fig. 8(b). The decomposed charge density at VB maximum, as seen in Fig. 8(c), shows an asymmetric distribution around each Pb atom with "lobes" pointing to the interstitial. These electronic structure features are similar to those of α-PbO [32,35,36]. The involvement of the nominally unoccupied Pb-6p orbitals of Pb(II) in VBs is essential to produce such an anisotropic charge distribution. Thus we find both hybridization between nominally unoccupied Pb 6p states and O 2p states, which reflects the lone pair activity of Pb(II), and the presence of antibonding Pb-6s/O-2p states at the top of the valence bands. This antibonding character is weaker, however, than that found in the corresponding Sn(II) compounds [6]. This is a consequence of the higher binding energy of the Pb 6s state relative to the Sn 5s state, due to the relativistic contraction of the s orbitals, as discussed above, and also in the context of orthorhombic PbO [37]. The antibonding character at the VB maximum is a feature that is associated with p-type dopability. While is there some antibonding character, clearly use of these compounds as transparent conductors will require an experimental study of the extent to which they can be doped.

It is useful to characterize the position of the valence band maximum relative to vacuum in order to assess the possibility of p-type doping [38–40]. For this purpose, we used supercell calculations for slabs of the different materials with a vacuum spacing of 20 Å, and a slab thickness of at least 14.9 Å, with an integer number of unit cells perpendicular to the layer direction. These calculations were done with the hybrid Heyd-Scuseria-Ernzerhof (HSE06) functional, with relaxation of the atomic coordinates in the slabs [41]. We find valence band maxima for Ca/$SrBaPb_2O_3$ and $BaPbO_2$ at -5.19, -5.16, -5.14, and -5.18 eV, respectively, with the zero at the potential in the middle of the vacuum. These values are comparable to known p-type oxides, e.g., -5.0 eV in Cu_2O [42], supporting the possibility that these new compounds may be doped p-type.

TABLE II. Estimated electrical conductivities (σ) at the indicated hole carrier concentration (p) for p-type Ca/Sr/$BaPb_2O_3$ and $BaPbO_2$ based on the calculated σ/τ and an assumed value of τ (see text) compared with the experimental values of typical p-type materials, $CuAlO_2$ [43] and SnO [44].

Material	p (cm^{-3})	σ ($S\,cm^{-1}$)
$CuAlO_2$ [43]	1.30×10^{17}	0.95×10^{-1}
SnO [44]	2.00×10^{20}	3.00×10^{2}
$CaPb_2O_3$	2.00×10^{20}	1.57×10^{2}
$SrPb_2O_3$	2.00×10^{20}	1.13×10^{2}
$BaPb_2O_3$	2.00×10^{20}	0.59×10^{2}
$BaPbO_2$	2.00×10^{20}	0.43×10^{2}

Table II shows calculated electrical conductivities (σ) at the selected hole carrier concentration (p) for p-type Ca/Sr/$BaPb_2O_3$ and $BaPbO_2$, compared with the experimental values of typical p-type materials $CuAlO_2$ [43] and SnO [44]. For these calculations, the assumed same concentration (p) and carrier relaxation time (τ) as those of SnO are adopted. The τ of SnO is evaluated with the experimental σ and our calculated σ/τ through the Boltzmann transport theory [27]. While the scattering rate will be sample dependent and is unknown, the measure shown, which assumes the same relaxation time for all materials, gives an indication of the favorability or otherwise of the band structure for conductivity. As seen, the theoretical σ of $CaPb_2O_3$ (157 $S\,cm^{-1}$), $SrPb_2O_3$ (113 $S\,cm^{-1}$), $BaPb_2O_3$ (59 $S\,cm^{-1}$), and $BaPbO_2$ (43 $S\,cm^{-1}$) are higher than that of $CuAlO_2$ (0.095 $S\,cm^{-1}$, at lower p), and comparable to the value (300 $S\,cm^{-1}$) of SnO. These results suggest that, if doped, these compounds have potential as conductive materials in the context of p-type TCOs and perhaps other applications.

IV. SUMMARY AND CONCLUSIONS

Motivated by the relative stability of Pb(II) compared to Sn(II) in oxides, we used structure prediction methods to search for ternary alkaline-earth metal Pb(II) oxides, $M_mPb_nO_{m+n}$ (M = Mg, Ca, Sr, and Ba), analogous to Sn(II) compounds. We identify four stable compounds, $CaPb_2O_3$ in the $Pccn$ structure, $SrPb_2O_3$ in the $Pccn$ structure, $BaPb_2O_3$ in the $Pca2_1$ structure, and $BaPbO_2$ in the $Pbca$ structure. These compounds show both lattice dynamical stability and thermodynamic stability with respect to competing phases. They all show wide band gaps, 2.99 eV for $CaPb_2O_3$, 3.09 eV for $SrPb_2O_3$, 2.86 eV for $BaPb_2O_3$, and 3.12 eV for $BaPbO_2$. $CaPb_2O_3$ and $SrPb_2O_3$ have moderate average m_h^*, $1.89m_0$ and $2.25m_0$, respectively. In contrast, $BaPb_2O_3$ and $BaPbO_2$ have heavier m_h^*, $4.70m_0$ and $6.46m_0$, respectively.

The family of ternary Pb(II) oxides containing alkaline/alkaline-earth metals follows Zintl behavior in that the alkaline-earth metal ions serve to supply electrons to the Pb(II)-O framework and occupy space. The stabilization of Ca/Sr/$BaPb_2O_3$ and $BaPbO_2$ in these systems can also be rationalized based on this Zintl concept. We find noticeable Pb-6s/O-2p antibonding character at the VBM, though weaker than in the Sn(II) compounds. This, plus the ternary Zintl-type nature of the compounds, may favor doping relative to the binary PbO. The reason is that the alkaline-earth metal site may offer a convenient place for doping because of the small contribution of alkaline-earth metal states to the active VBs, and the ionic nature of these atoms. For example, alkaline-earth metal vacancies or substitutions by monovalent ions may be p-type dopants. The possibility of the existence of compensating intrinsic defects (i.e., hole killers) such as Pb interstitials and oxygen vacancies should be considered in the context of doping studies if these compounds are successfully synthesized. These compounds contain Pb, which, depending on the intended application, may be undesirable. Compared to the Sn(II) phases that have been studied as potential TCOs, the Pb(II) phases are more stable, but may be more difficult to dope. It will be of interest to verify these phases by experimental synthesis, and, if successful, to experimentally measure the electronic and optical properties and attempt doping.

ACKNOWLEDGMENTS

This work was supported in part by the Department of Energy, Basic Energy Sciences, Computational Materials Sciences Program, through the MAGICS center Award No. DE-SC0014607 (crystal structure search by Y.L.), and in part by the S3TEC Energy Frontier Research Center, Award No. DE-SC0001299/DE-FG02-09ER46577 (properties, D.J.S.). Work at Jilin University was supported by National Natural Science Foundation of China (under Grants No. 11404131 and No. 11674121) and the Special Fund for Talent Exploitation in Jilin Province of China.

[1] A. L. Allred and E. Rochow, J. Inorg. Nucl. Chem. **5**, 269 (1958).
[2] M. W. Chase, Jr., *NIST-JANAF Thermochemical Tables*, 4th ed., J. Phys. Chem. Ref. Data Monograph 9 (ACS/AIP, New York, 1998), p. 1.
[3] J. D. Cox, D. D. Wagman, and V. A. Medvedev, *CODATA Key Values for Thermodynamics* (Hemisphere, New York, 1984).
[4] R. M. Braun and R. Hoppe, Angew. Chem., Int. Ed. Engl. **17**, 449 (1978).
[5] R. M. Braun and R. Hoppe, Z. Naturforsch. B **37**, 688 (1982).
[6] Y. Li, D. J. Singh, M.-H. Du, Q. Xu, L. Zhang, W. Zheng, and Y. Ma, J. Mater. Chem. C **4**, 4592 (2016).
[7] S. M. Woodley and R. Catlow, Nat. Mater. **7**, 937 (2008).
[8] Y. Wang, J. Lv, L. Zhu, and Y. Ma, Phys. Rev. B **82**, 094116 (2010).
[9] Y. Wang, J. Lv, L. Zhu, and Y. Ma, Comput. Phys. Commun. **183**, 2063 (2012).
[10] Z. Zhao, B. Xu, X.-F. Zhou, L.-M. Wang, B. Wen, J. He, Z. Liu, H.-T. Wang, and Y. Tian, Phys. Rev. Lett. **107**, 215502 (2011).

[11] X. Zhang, Y. Wang, J. Lv, C. Zhu, Q. Li, M. Zhang, Q. Li, and Y. Ma, J. Chem. Phys. **138**, 114101 (2013).
[12] M. Zhang, H. Liu, Q. Li, B. Gao, Y. Wang, H. Li, C. Chen, and Y. Ma, Phys. Rev. Lett. **114**, 015502 (2015).
[13] Q. Wang, B. Xu, J. Sun, H. Liu, Z. Zhao, D. Yu, C. Fan, and J. He, J. Am. Chem. Soc. **136**, 9826 (2014).
[14] G. Kresse and D. Joubert, Phys. Rev. B **59**, 1758 (1999).
[15] G. Kresse and J. Furthmüller, Phys. Rev. B **54**, 11169 (1996).
[16] J. P. Perdew, K. Burke, and M. Ernzerhof, Phys. Rev. Lett. **77**, 3865 (1996).
[17] A. Togo and I. Tanaka, Scr. Mater. **108**, 1 (2015).
[18] F. Tran and P. Blaha, Phys. Rev. Lett. **102**, 226401 (2009).
[19] D. Koller, F. Tran, and P. Blaha, Phys. Rev. B **83**, 195134 (2011).
[20] D. J. Singh, Phys. Rev. B **82**, 155145 (2010).
[21] Y.-S. Kim, M. Marsman, G. Kresse, F. Tran, and P. Blaha, Phys. Rev. B **82**, 205212 (2010).
[22] D. J. Singh, Phys. Rev. B **82**, 205102 (2010).
[23] D. J. Singh and L. Nordstrom, *Planewaves, Pseudopotentials, and the LAPW Method*, 2nd ed. (Springer, Berlin, 2006).
[24] P. Blaha, K. Schwarz, G. Madsen, D. Kvasnicka, and J. Luitz, *WIEN2k, An Augmented Plane Wave+Local Orbitals Program for Calculating Crystal Properties* (Karlheinz Schwarz, Technische Universität Wien, Austria, 2001).
[25] K. Balasubramanian, J. Phys. Chem. **93**, 6585 (1989).
[26] K. Hummer, A. Grüneis, and G. Kresse, Phys. Rev. B **75**, 195211 (2007).
[27] G. K. H. Madsen and D. J. Singh, Comput. Phys. Commun. **175**, 67 (2006).
[28] See Supplemental Material at http://link.aps.org/supplemental/10.1103/PhysRevMaterials.1.055001 for data for metastable phases.
[29] T. F. Fässler, *Zintl Phases: Principles and Recent Developments*, Vol. 139 (Springer, Berlin, 2011).
[30] G. Xing, J. Sun, K. P. Ong, X. Fan, W. Zheng, and D. J. Singh, APL Mater. **4**, 053201 (2016).
[31] J. Yang, L. Xi, W. Qiu, L. Wu, X. Shi, L. Chen, J. Yang, W. Zhang, C. Uher, and D. J. Singh, npj Comput. Mater. **2**, 15015 (2016).
[32] H. J. Terpstra, R. A. de Groot, and C. Haas, Phys. Rev. B **52**, 11690 (1995).
[33] G. Hautier, A. Miglio, G. Ceder, G.-M. Rignanese, and X. Gonze, Nat. Commun. **4**, 2292 (2013).
[34] R. Hoffman, *Solids and Surfaces* (Wiley-VCH, New York, 1988), p. 42.
[35] G. Trinquier and R. Hoffmann, J. Phys. Chem. **88**, 6696 (1984).
[36] G. W. Watson, S. C. Parker, and G. Kresse, Phys. Rev. B **59**, 8481 (1999).
[37] M. Liao, S. Takemoto, Z. Xiao, Y. Toda, T. Tada, S. Ueda, T. Kamiya, and H. Hosono, J. Appl. Phys. **119**, 165701 (2016).
[38] A. Zunger, Appl. Phys. Lett. **83**, 57 (2003).
[39] A. Walsh, C. R. A. Catlow, R. Galvelis, D. O. Scanlon, F. Schiffmann, A. A. Sokol, and S. M. Woodley, Chem. Sci. **3**, 2565 (2012).
[40] A. Walsh and K. T. Butler, Acc. Chem. Res. **47**, 364 (2014).
[41] J. Heyd, G. E. Scuseria, and M. Ernzerhof, J. Chem. Phys. **118**, 8207 (2003).
[42] S. Mukherjee, R. Maiti, A. K. Katiyar, S. Das, and S. K. Ray, Sci. Rep. **6**, 29016 (2016).
[43] H. Kawazoe, M. Yasukawa, H. Hyodo, M. Kurita, H. Yanagi, and H. Hosono, Nature (London) **389**, 939 (1997).
[44] A. Behrendt, C. Friedenberger, T. Gahlmann, S. Trost, T. Becker, K. Zilberberg, A. Polywka, P. Görrn, and T. Riedl, Adv. Mater. **27**, 5961 (2015).